Journal of Sound and Vibration (1993) **166**(1), 55–76

STRUCTURE-BORNE SOUND TRANSMISSION AT ELASTICALLY CONNECTED PLATES

P. MEES AND G. VERMEIR

Laboratory of Building Physics, Department of Civil Engineering, KULeuven, Celestijnenlaan 131, *B*-3001 *Leuven (Heverlee), Belgium*

(*Received* 1 *October* 1991, *and in final form* 24 *March* 1992)

The bending wave transmission between semi-infinite thin plates connected by a hinge or by an elastic interlayer is analyzed. The wave transmission across the interlayer is calculated analytically; the stiffening effect of the interlayer is simulated with a finite element model. The calculation results for the bending wave transmission demonstrate the importance of an offset mounting of a plate, and of the modulus of elasticity, the Poisson ratio, the loss factor and the shape of the interlayer. Theoretical predictions are compared with experimental results for a hinge and for different elastic interlayers in a T-junction.

1. INTRODUCTION

The modelling of structure-borne energy flow at junctions is an important topic in the study of mechanical vibrations of structures. These junctions can constitute a change in cross-section, material or direction of the parts of the structure. One method of modelling the energy flow at junctions is to describe the vibration of the structure by means of different wave types propagating in the parts of the structure. In this approach, the energy flow through a junction is quantified by its reflection and its transmission coefficients, respectively defined as the ratio of the reflected or transmitted intensity carried by any wave type to the intensity incident on the junction [1]. The aim is then to calculate the different coefficients from the dynamic characteristics of the junction and the parts of the structure. In this paper, the wave approach is applied to the case of structure-borne sound transmission for plates of semi-infinite extent connected by a hinge or by an elastic interlayer.

The reflection and transmission coefficients of junctions between semi-infinite plates have been calculated by several authors [1–12]. Cremer *et al.* [1] analyzed longitudinal and bending wave transmission at normal incidence for different junctions, as well as bending wave transmission for oblique incidence at a corner junction. They also studied the attenuation of longitudinal and bending waves by an elastic interlayer between plates, for the case of normal incidence. Kihlman [2] calculated bending wave transmission at symmetric cross junctions for the case of random incidence. The general case of the transmission of the three wave types (bending waves, longitudinal waves and transverse waves) at random incidence, for arbitrary L, T and cross junctions was elaborated by Wöhle, Beckmann and Schreckenbach [3, 4] and by Craven and Gibbs [5, 6]. Wöhle, Beckmann and Schreckenbach [3] also mentioned the possibility of introducing elastic connections between the plates, and demonstrated the influence of a rotational compliance of the junction on sound transmission in buildings [7]. Several studies [8–13] developed refinements of these basic theories. Gibbs [8] presented a detailed analysis of wave type conversion in a series of T-junctions of plates. Leung and Pinnington [9] investigated

0022-460X/93/190055 + 22 $08.00/0

longitudinal and bending wave transmission at a rectangular junction with a spring-dashpot compliance, both in rotation and translation, for the case of normal incidence. Gudmundsson [10] investigated both analytically and experimentally the wave transmission between two horizontal plates connected by an elastic interlayer. He also modelled the interlayer as a spring-dashpot compliance. Rosenhouse and Mechel [11] investigated the influence of a hinge on bending wave transmission between plates. Langley and Heron [12] considered a junction which consists of an arbitrary number of plates coupled through a beam or directly coupled along a line. McCollum and Cuschieri [13] calculated power transmission at an L-shaped junction including both the effects of in-plane waves and rotary inertia and shear (Mindlin bending) in the plates. Finally, several studies of wave propagation through beam-like structures [14–18] contain results that can be applied to the case of wave transmission at normal incidence in plate-like structures. Kurtze, Tamm and Vogel [14] presented detailed experimental results on the transmission of bending waves at a corner junction between rods with rigid, elastic and hinged junctions. Several authors [15–18] have analyzed the influence of bends and joints on the energy flow and wave type conversion in beams, including a precise modelling of the rigid junction as an element with a certain dimension, mass or rigidity [17, 18].

The purpose of this paper is to analyze structure-borne sound transmission between plates connected by a hinge or by an elastic interlayer. The wave approach is used and the study is limited to the transmission of a structure-borne bending wave incident on a junction of thin plates of semi-infinite extent. First, the procedure to calculate the wave transmission is reviewed. This includes the description of the three wave types in the plates and a general formulation of the boundary conditions at the junction. Second, two boundary conditions at the junction are considered in more detail. A hinge is modelled as a junction without rotational stiffness and with an offset with respect to the centrelines of the plates. An elastic interlayer between two plates is modelled as a junction with compliance in both rotation and translation. Special attention is paid to the modelling of the dynamic behaviour of the interlayer. Both an analytical model, based on the wave transmission, and a numerical model, based on the finite element method, are considered. The influence of the different junction parameters is illustrated by selected calculation examples. Finally, experimental results for a T-junction between plates are compared with theoretical predictions. Both rigid, hinged and elastic connections between the plates are included in the experiment.

2. MODEL OF THE JUNCTION

The geometry considered in this paper is shown in Figure 1. Four plates of semi-infinite extent are joined at a common line by means of a junction beam. T- or L-junctions are obtained by omitting one or two plates from this scheme. The junction beam is introduced to facilitate the description of the boundary conditions at the junction; it is an element without mass or rigidity, and its dimensions are characterized by an offset e_p by which a plate is mounted at the junction. The calculations presented in the paper are limited to the case of an incident bending wave. This restriction was imposed because experimental verification is most easy for this case. No complications arise when treating the case of an incident in-plane quasi-longitudinal or transverse wave.

The analysis of the wave transmission follows the work of Wöhle, Beckmann and Schreckenbach [3, 4] and Craven and Gibbs [5, 6], so only the essential formulations will be given here. A structure-borne bending wave is incident from plate 1 on the junction. The excitation is assumed to be harmonic, with time dependence $e^{j\omega t}$. No restrictions are imposed on the motion of the junction, so in general a bending wave and an in-plane

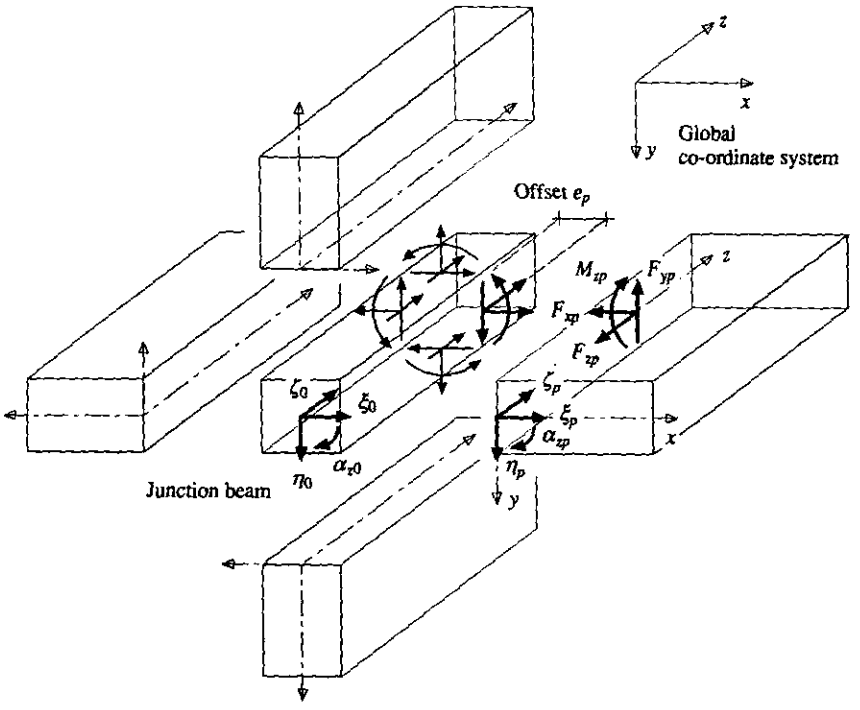

Figure 1. Geometry, displacements and forces for a rigid junction.

quasi-longitudinal and transverse wave propagate from the junction in each plate. These three wave types all have the same z-dependency as imposed by the incident bending wave. The plates are assumed to be homogeneous, isotropic and thin compared to the bending wavelength. For the plate material, no internal losses are taken into account. The propagation of bending waves is governed by the Kirchhoff plate equation; the solution for the plate displacement η_p and rotation α_p contains two unknown amplitudes A_p and B_p. The propagation of in-plane waves is governed by the equation for longitudinal and transverse waves for the case of plane stress in the y-direction; the solution for the plate displacements ξ_p and ζ_p contains two unknown amplitudes C_p and D_p. The forces F_{xp}, F_{yp} and F_{zp} and the bending moment M_{zp} at the edge of the plate, required to construct the boundary conditions, follow from the plate displacements by using the formulae of mechanics. The final set of unknowns includes the complex displacement amplitudes A_p, B_p, C_p and D_p for each plate and the complex displacement amplitudes ξ_0, η_0, ζ_0 and α_{z0} of the junction beam. These unknowns are determined from the continuity and equilibrium conditions at the junction.

In a rigid junction (see Figure 1), the plates are rigidly connected to the junction beam. In this case, the displacements at the edge of the plate are equal to the displacements of the junction beam, and the forces and the bending moment at the edge of the plate act directly on the junction beam. Consequently, for each plate, four continuity conditions can be written in the local co-ordinate system of the plate (a list of symbols is given in Appendix 2):

$$\xi_p = \xi_0 \cos\theta_p + \eta_0 \sin\theta_p, \qquad \eta_p = -\xi_0 \sin\theta_p + \eta_0 \cos\theta_p + e_p \alpha_{z0}, \tag{1, 2}$$

$$\zeta_p = \zeta_0, \qquad \alpha_{zp} = \alpha_{z0}. \tag{3, 4}$$

For the junction beam, four equilibrium conditions can be written in the global co-ordinate system of the junction:

$$\sum_p (F_{xp} \cos \theta_p - F_{yp} \sin \theta_p) = 0, \qquad \sum_p (F_{xp} \sin \theta_p + F_{yp} \cos \theta_p) = 0, \tag{5, 6}$$

$$\sum_p F_{zp} = 0, \qquad -\sum_p M_{zp} + \sum_p e_p F_{yp} = 0. \tag{7, 8}$$

In equations (1)–(8), the displacements, forces and bending moment are evaluated at the edge of the plate, at $x = 0$. θ_p is the angle of inclination of a plate with respect to the x–y axes of the global co-ordinate system. As can be seen from equations (2) and (8), the effect of a mounting offset e_p is to introduce a supplementary displacement component and a supplementary contribution to the bending moment acting on the junction beam. For the case of a rigid junction, it is difficult to attribute a physical meaning to this offset e_p because the transition from one plate to another is not well defined. One could introduce it to account for the case of a rigid junction with plates that do not intersect at a common line, or with plates that are joined through a beam of finite dimensions. This kind of geometry, as used for instance by Langley and Heron [12], is not considered in this study. Consequently, the offset is taken to be zero for a rigid junction. For the case of a junction with a hinge or with an elastic interlayer, the location of a plate's edge is more easy to define. In these cases an offset can be included to account for the position of the hinge or the elastic interlayer with respect to the other plates.

The statements (1)–(8) constitute a set of linear equations, the solution of which yields the amplitudes that determine the motion of the plates and of the junction beam. The transmission coefficient τ_p for the bending wave from plate 1 to plate p is the ratio of the transmitted bending wave intensity to the incident bending wave intensity. The average transmission coefficient $\bar{\tau}_p$ is calculated by integrating over all angles of incidence of the primary bending wave, or up to the angle of total reflection. Finally, the bending wave transmission loss R_p is calculated as

$$R_p = -10 \log (\bar{\tau}_p). \tag{9}$$

Results for the rigid junction are similar to results from the literature, so no calculations will be presented for this case. The theory for the rigid junction serves only as a reference for the other junction conditions. It has to be noted that in the cases of both the hinged and the elastic junction, at least one plate of the assembly should be rigidly connected to the junction beam.

3. HINGED JUNCTION

In many cases, the junctions between plates can be assumed to be rigid connections. In some cases however, this ideally rigid boundary condition is not satisfied, and other types of connections should be considered. Because of the complexity of real junctions, simplifying assumptions must be made in their mechanical description. A hinge can be introduced to characterize a junction with an incomplete contact between the plates, which results in a negligible transfer of bending moments compared to the transfer of shear forces. In a building structure, for instance, a hinge can be a first approximation for a junction between plates where small cracks developed at the junction line due to static deformations, or for a junction between prefabricated plates that was not properly filled up after assembly. It is likely that in many situations the hinge is not located exactly at the centreline of the junction. This can be accounted for by an offset e_p of the hinge with respect to the centreline of the junction beam. In this study, the location of the hinge is taken to be symmetric, at

the centre of the plate's edge; consequently only an offset in the x-direction is considered. Due to the perfect rotational compliance of the hinge, the bending moment at the edge of each plate with a hinge vanishes:

$$M_{zp}=0 \qquad \text{for plate } p \text{ hinged.} \tag{10}$$

The set of equations for the hinged junction is now obtained from the statements (1)–(8), by replacing equation (4) with equation (10), and applying equation (10) in the moment equilibrium (8).

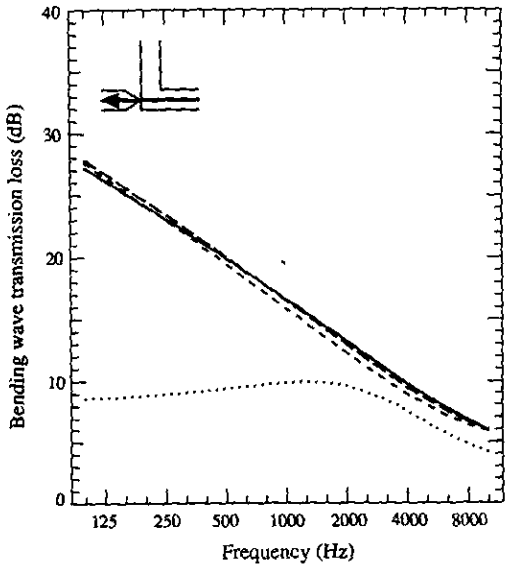

Figure 2. Predicted transmission loss for a coplanar hinge. Hinge offset relative to plate thickness: - - - -, offset 0; – – –, offset 1/4; ——, offset 1/2; · · · ·, rigid junction.

The influence of a hinge on the bending wave transmission is illustrated in Figures 2 and 3. The example concerns a T-junction where, alternatively, the second or the third plate are connected to the junction beam by means of a hinge. In both cases, the attenuation provided by the hinge decreases with increasing frequency. This is because of the lateral displacement of the plate, causing the bending wave transmission, becomes easier for higher frequencies. The influence of an offset mounting of the hinge is most marked in the case of corner transmission (see Figure 3). In this case, a zero offset leads to a nearly infinite transmission loss (graph not shown on the figure), and the transmission loss decreases for an increasing offset. In practical applications, a hinge offset of half the plate's thickness should be a realistic value.

4. ELASTIC JUNCTION

In the case of an elastic junction, one or more plates are connected to the junction beam by means of an elastic coupling element. In general, such an element can be characterized by an arbitrary compliance in translation and in rotation. This approach, as used, for instance, by Leung and Pinnington [9], has the advantage of clearly demonstrating the influence of a compliance in one specific direction. In many situations, however, compliances in different directions will be found in combined form, which makes it necessary to determine their values simultaneously from the geometrical and material characteristics of the coupling element. The present study is limited to the case of a layer of isotropic elastic

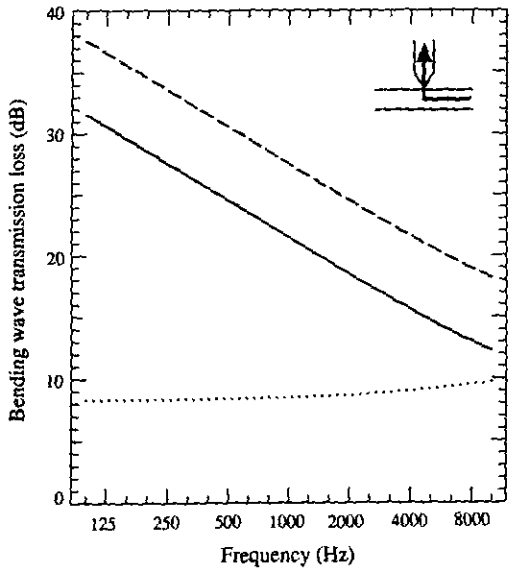

Figure 3. Predicted transmission loss for a corner hinge. Hinge offset relative to plate thickness: – – –, offset 1/4; ——, offset 1/2; · · · ·, rigid junction.

material introduced over the whole coupling length between a plate and the junction beam (see Figure 4). In a building, for instance, such an elastic interlayer could be selectively introduced between plates to increase the sound insulation between rooms. The interlayer has a thickness d_l and a width equal to the thickness h_p of the plate connected to it. The interlayer material is characterized by its modulus of elasticity E_l and its Poisson ratio ν_l. Its material damping is characterized by an internal loss factor η_l and is accounted for in the calculations by a complex modulus of elasticity. The Poisson ratio is assumed to be a

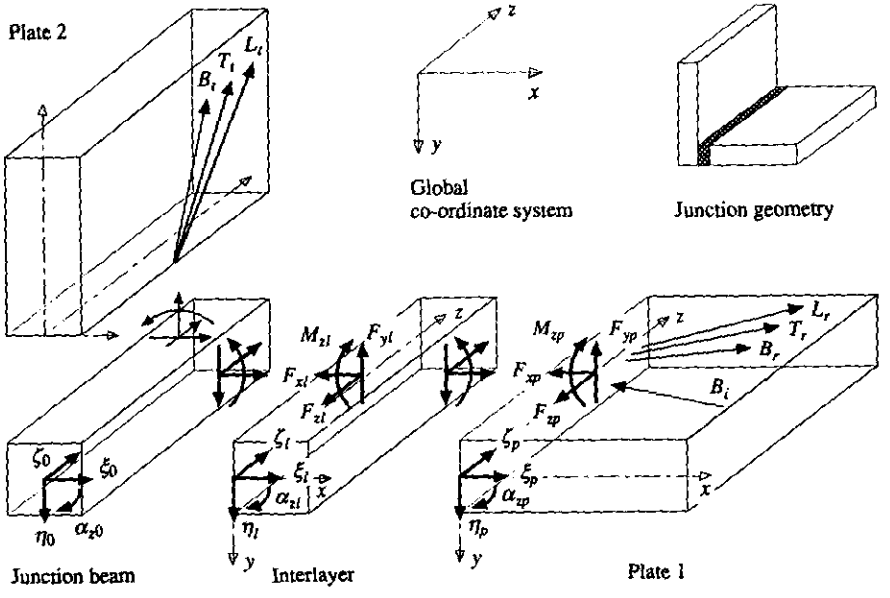

Figure 4. Geometry, displacements and forces for a junction with an elastic interlayer.

real quantity. As in the case of a hinged junction, it is likely that in many situations, the interlayer is not located exactly at the centreline of the junction. When a wall, for instance, is mounted on a floor with an elastic interlayer introduced between both, the edge of the interlayer in contact with the floor is at an offset of half the floor's thickness. In this case, only an x-direction offset has a physical meaning.

The continuity and equilibrium equations governing the bending wave transmission are similar to the equations (1)–(8) for the case of a rigid junction. When a plate is connected to the junction beam by means of an elastic interlayer, one only needs to replace the quantities at the edge of a plate (index p) by the corresponding quantities at the edge of the interlayer (index l). In this way, eight new quantities are introduced for each interlayer l (see Figure 4):

$$[L]^T = [\xi_l \quad \zeta_l \quad F_{xl} \quad F_{zl} \quad \eta_l \quad F_{yl} \quad \alpha_{zl} \quad M_{zl}]. \tag{11}$$

These quantities $[L]$ represent no new unknowns, but they can be expressed in terms of the corresponding quantities at the edge of the plate p connected to the interlayer,

$$[P]^T = [\xi_p \quad \zeta_p \quad F_{xp} \quad F_{zp} \quad \eta_p \quad F_{yp} \quad \alpha_{zp} \quad M_{zp}], \tag{12}$$

where the relation between both sets has the form

$$[L] = [T][P]. \tag{13}$$

$[T]$ is an 8×8 complex matrix, which describes the transfer of displacements and forces from the edge $x = 0$ of the plate to the edge $x = 0$ of the interlayer. This procedure allows one to keep the same set of unknown amplitudes A_p, B_p, C_p, D_p, ξ_0, η_0, ζ_0 and α_{z0} as in the case of the rigid junction. After solution for the unknowns, the displacements and forces at the edge $x = 0$ of the interlayer can be calculated by using equation (13). The final calculations for the transmission loss are similar to the case of a rigid junction.

In the case of an elastic junction, the key point is the calculation of the interlayer transfer matrix $[T]$. This matrix is fully determined by the material characteristics and the geometry of the interlayer. However, for its calculation, simplifying assumptions must be made regarding the dynamics of the interlayer.

In a first approximation, the interlayer can be considered as a spring-dashpot system. In this case, the forces and bending moment on both sides of the interlayer are equal:

$$F_{xl} = F_{xp}, \qquad F_{yl} = F_{yp}, \qquad F_{zl} = F_{zp}, \qquad M_{zl} = M_{zp}. \tag{14}$$

If the displacement components ξ, η and ζ and the rotation α_z are assumed to vary linearly with x across the interlayer, then the forces and bending moment at both sides of the interlayer are proportional to the differences in displacement, as follows:

$$F_{xl} = -\frac{E_l(1-\nu_l)}{(1+\nu_l)(1-2\nu_l)} \frac{h_p}{d_l} (\xi_l - \xi_p), \qquad F_{yl} = -\frac{E_l}{2(1+\nu_l)} \frac{h_p}{d_l} (\eta_l - \eta_p),$$

$$F_{zl} = -\frac{E_l}{2(1+\nu_l)} \frac{h_p}{d_l} (\zeta_l - \zeta_p), \qquad M_{zl} = \frac{E_l(1-\nu_l)}{(1+\nu_l)(1-2\nu_l)} \frac{h_p^3}{12 d_l} (\alpha_{zl} - \alpha_{zp}). \tag{15}$$

Equations (14) and (15) completely determine the transfer matrix $[T]$. The resulting elements of the matrix $[T]$ are given in Appendix 1. In equations (15) it has been assumed that the interlayer displacements and rotation do not vary with y and z. This assumption is valid for the limiting case of an infinitely long interlayer, with a small thickness d_l compared to its width h_p, and with its endplanes rigidly attached to the junction beam and to the edge of a plate. Alternatively, it could be assumed that the infinitely long interlayer can expand and contract freely in the y direction, perpendicular to the plate

surface, without friction at its endplanes. With this assumption, the expressions for F_{xl} and M_{zl} in equations (15) are as follows:

$$F_{xl} = -\frac{E_l}{1-\nu_l^2}\frac{h_p}{d_l}(\xi_l - \xi_p), \qquad M_{zl} = \frac{E_l}{1-\nu_l^2}\frac{h_p^3}{12 d_l}(\alpha_{zl} - \alpha_{zp}). \tag{16}$$

In a more exact theory, wave propagation in the interlayer should be taken into account. Wave propagation can become important at high frequencies, for interlayers with a thickness d_l large compared to the longitudinal and transverse wavespeed in the interlayer material. It is assumed that four wave types propagate in the interlayer: a quasi-longitudinal and transverse wave with displacements parallel to the plane of the plate, a transverse wave with a plane displacement of the cross-section perpendicular to the plane of the plate, and a plane rotation of the cross-section.

The in-plane waves in the isotropic interlayer can be expressed in terms of a potential Φ_l and a scalar stream function Ψ_l [1]. These satisfy the equations for, respectively, the propagation of longitudinal and transverse waves in an infinite medium:

$$\Delta\Phi_l + k_{Ll}^2\Phi_l = 0, \qquad \Delta\Psi_l + k_{Tl}^2\Psi_l = 0. \tag{17}$$

The solutions for the longitudinal and transverse waves in the interlayer are

$$\begin{aligned}\Phi_l(x,z) &= (C_l^+ \, e^{-jk_{Llx}x} + C_l^- \, e^{+jk_{Llx}x}) \, e^{-jk_{Bl}\sin\theta_1 z},\\ \Psi_l(x,z) &= (D_l^+ \, e^{-jk_{Tlx}x} + D_l^- \, e^{+jk_{Tlx}x}) \, e^{-jk_{Bl}\sin\theta_1 z}.\end{aligned} \tag{18}$$

In equations (18), k_{Llx} and k_{Tlx} are the wavenumber components for the longitudinal and the transverse wave propagation in the x-direction normal to the junction line. These wavenumbers are determined by Snell's law for the refraction of the incident bending wave:

$$k_{Llx} = \sqrt{k_{Ll}^2 - k_{Bl}^2\sin^2\theta_1}, \qquad k_{Tlx} = \sqrt{k_{Tl}^2 - k_{Bl}^2\sin^2\theta_1}. \tag{19}$$

The in-plane displacements ξ_l and ζ_l along the x- and z-axes are obtained as

$$\xi_l = \partial\Phi_l/\partial x - \partial\Psi_l/\partial z, \qquad \zeta_l = \partial\Phi_l/\partial z + \partial\Psi_l/\partial x. \tag{20}$$

The plane transverse displacement η_l and the plane rotation α_{zl} satisfy, respectively, the equation for the propagation of transverse and longitudinal waves:

$$\Delta\eta_l + k_{Tl}^2\eta_l = 0, \qquad \Delta\alpha_{zl} + k_{Ll}^2\alpha_{zl} = 0. \tag{21}$$

The solutions for the plane transverse displacement and the plane rotation in the interlayer are

$$\begin{aligned}\eta_l(x,z) &= (A_l^+ \, e^{-jk_{Tlx}x} + A_l^- \, e^{+jk_{Tlx}x}) \, e^{-jk_{Bl}\sin\theta_1 z},\\ \alpha_{zl}(x,z) &= (B_l^+ \, e^{-jk_{Llx}x} + B_l^- \, e^{+jk_{Llx}x}) \, e^{-jk_{Bl}\sin\theta_1 z}.\end{aligned} \tag{22}$$

For the case of a lossless plate connected to a lossless interlayer, the motion for a particular wave type consists either of a propagating wave or of an exponentially decaying wave. The transition occurs at the angle of total reflection of the incident bending wave for that particular wave type. For the case of an interlayer material with internal damping, this clear distinction cannot be made. In this case, the modulus of elasticity of the interlayer material is complex, resulting in complex longitudinal and transverse wavenumbers k_{Ll} and k_{Tl}. The wavenumber component parallel to the junction line is real, since it equals the real trace wavenumber imposed by the infinitely wide bending wavefront incident on the infinitely long junction line. For all angles of incidence, the wavenumber components

k_{Llx} and k_{Tlx} in the x-direction normal to the junction line, given by equation (19), have a (positive) real as well as a (negative) imaginary part. The transition at the angle of total reflection of the incident bending wave now results in the interlayer wave type being "predominantly propagating" or "predominantly decaying". The case in which both the plate and the interlayer material are damped is not considered in this study. The calculations could be performed without difficulties by using complex wavenumbers for all the wavefields. However, as discussed by Craven and Gibbs [5], a problem arises regarding the calculation and the interpretation of the transmitted and reflected intensities in the plates.

In order to formulate the boundary conditions at the junction, with the conventions as indicated in Figure 4, the forces and the bending moment in the interlayer are calculated as follows:

$$F_{xl}=\frac{E_l(1-\nu_l)}{(1+\nu_l)(1-2\nu_l)}h_p\left(\frac{\partial\xi_l}{\partial x}+\frac{\nu_l}{1-\nu_l}\frac{\partial\zeta_l}{\partial z}\right), \qquad F_{yl}=\frac{E_l}{2(1+\nu_l)}h_p\frac{\partial\eta_l}{\partial x},$$

$$F_{zl}=\frac{E_l}{2(1+\nu_l)}h_p\left(\frac{\partial\zeta_l}{\partial x}+\frac{\partial\xi_l}{\partial z}\right), \qquad M_{zl}=-\frac{E_l(1-\nu_l)}{(1+\nu_l)(1-2\nu_l)}\frac{h_p^3}{12}\frac{\partial\alpha_{zl}}{\partial x}. \tag{23}$$

In equations (23), the same assumptions have been made as discussed after equations (15). The transfer matrix $[T]$ can now be constructed by evaluating the displacements, rotation, forces and bending moment at both edges $x=0$ and $x=d_l$ of the interlayer, followed by eliminating the amplitudes A_l, B_l, C_l and D_l. This is a procedure similar to the construction of transfer matrices for the propagation of waves in layered media [19]. The resulting elements of the matrix $[T]$ are given in Appendix 1.

In Figures 5–9, calculated results are presented for a T-junction with rigidly connected coplanar plates and an elastically connected third plate. The characteristics of the plates are $d_p=10$ mm, $\rho_p=1440$ kg/m^3 and $E_p=3580$ MPa; the characteristics of the interlayer are $d_l=2$ mm, $\rho_l=1050$ kg/m^3 and $E_p=2{\cdot}5$ MPa. All the calculations were performed with the stress–strain relationships for the interlayer as assumed in equations (23).

In Figure 5 are shown the general characteristics of the bending wave transmission loss as well as the influence of an offset mounting of the interlayer. The coplanar bending wave transmission is not influenced by the offset mounting. The shear force at the interlayer edge and the corresponding bending moment caused by the offset mounting (second term in equation (8)), are too small to influence the dynamic moment equilibrium of the rigid coplanar junction. The transmission loss has a maximum in the frequency range where the magnitude of the longitudinal impedance of the interlayer matches the magnitude of the point impedance in the middle of the crossing plates [9]. Above this frequency, the transverse motion of the coplanar plates become decoupled from the in-plane motion of the third plate, resulting in a perfect bending wave transmission. The corner bending wave transmission across the interlayer is strongly influenced by an offset mounting of the layer. If a zero offset is assumed, bending wave transmission results from a moment transfer across the interlayer. The resulting transmission loss is relatively high, because the rotational stiffness of the layer is low compared to its translational stiffness. The bending wave transmission loss has a maximum in the frequency range where the magnitude of the shear impedance of the interlayer matches the magnitude of the point impedance on the edge of plate 3 [9]. In the case of a non-zero offset, a rotation of the junction also causes a transverse displacement of the interlayer endplane at $x=0$, and a supplementary bending wave transmission results from the transfer of shear forces across the interlayer. This results in a considerably lower transmission loss compared with the case of a zero offset. Moreover, the transmission loss now shows a minimum at the first shear resonance across

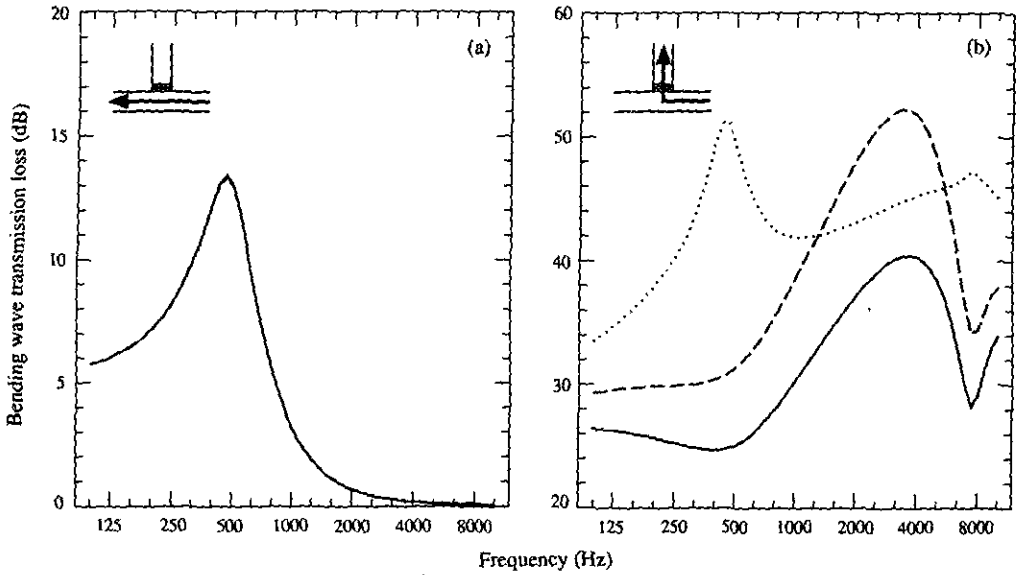

Figure 5. Predicted transmission loss for an elastic junction. Offset relative to plate thickness: · · · ·, offset 0; – – –, offset 1/4; ——, offset 1/2.

the thickness of the interlayer, when the shear wavelength equals twice the interlayer thickness.

The influence of the Poisson ratio of the interlayer material on the bending wave transmission loss is shown in Figures 6 and 7. When using the equations (23) for a thin interlayer, Poisson's ratio is an important parameter since the apparent compression stiffness of an isotropic interlayer, given by $E(1-\nu)/(1+\nu)(1-2\nu)$, becomes very high for materials with a value of ν approaching 0·5. In Figure 6, the influence is shown for the case of a zero offset of the interlayer. An increasing Poisson ratio increases the longitudinal

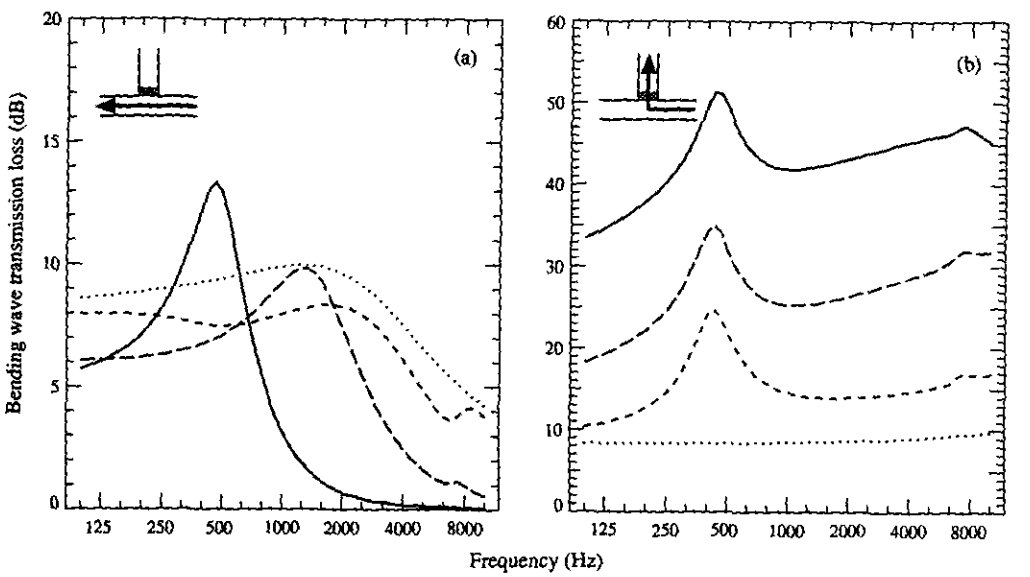

Figure 6. Predicted transmission loss for an elastic junction without offset. Interlayer Poisson ratio: - - - - -, $\nu_l = 0{\cdot}499$; – – –, $\nu_l = 0{\cdot}49$; ——, $\nu_l = 0{\cdot}4$; · · · ·, rigid junction.

impedance of the interlayer, and shifts the maximum in the coplanar transmission loss to higher frequencies. At the same time, this maximum is spread out over a larger frequency range. In the limit of ν approaching 0·5, only the shear stiffness of the interlayer remains finite. The coplanar transmission loss then almost approaches the value for the case of a rigid junction. An increasing Poisson ratio also increases the rotational stiffness of the interlayer, and therefore increases the corner bending wave transmission across the interlayer. The location of the maximum in the corner junction damping, associated with the shear stiffness of the interlayer, remains almost unchanged. In Figure 7, the influence is

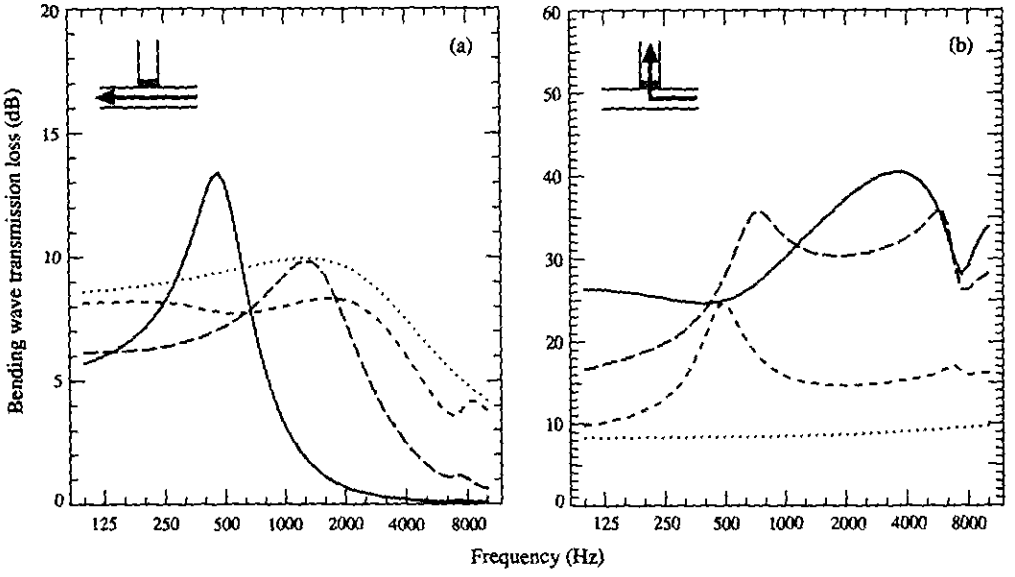

Figure 7. Predicted transmission loss for an elastic junction with an offset of 1/2 the plate's thickness. Interlayer Poisson ratio: - - - - -, $\nu_l = 0{\cdot}499$; – – –, $\nu_l = 0{\cdot}49$; ——, $\nu_l = 0{\cdot}4$; · · · ·, rigid junction.

shown for the case of a non-zero offset of the interlayer. The coplanar transmission loss has the same values as plotted for the centred case (Figure 6(a)). With an increasing Poisson ratio, the value for the corner bending wave transmission loss across the interlayer gradually approaches the value for the zero offset. The shear stiffness of the interlayer remains unchanged, whereas its rotational stiffness increases. Therefore, the faction of the bending wave transmission resulting from the moment transfer across the interlayer increases compared to the fraction resulting from the transfer of shear forces. In the limit of ν approaching 0·5, both the non-zero and the zero offset case yield the same result, approaching the value for the case of a rigid junction.

The influence of the loss factor of the interlayer material on the bending wave transmission loss, for the case of a non-zero offset of the interlayer, is shown in Figure 8. For the coplanar bending wave transmission, the maximum of the transmission loss is slightly decreased and spread out when the loss factor increases. For the corner bending wave transmission, the minimum of the transmission loss at the shear resonance is increased. The fraction of the incident bending wave intensity that is absorbed in the interlayer is shown in Figure 9. For the case of a lossless interlayer, the sum of the transmission and reflection coefficients of the incident bending wave into the three wave types in the three plates equals one (zero if expressed logarithmically as in Figure 9). For the case of an interlayer with internal damping, this sum is always less than one, and decreases with increasing loss factor. The values in Figure 9 illustrate that the energy losses in the

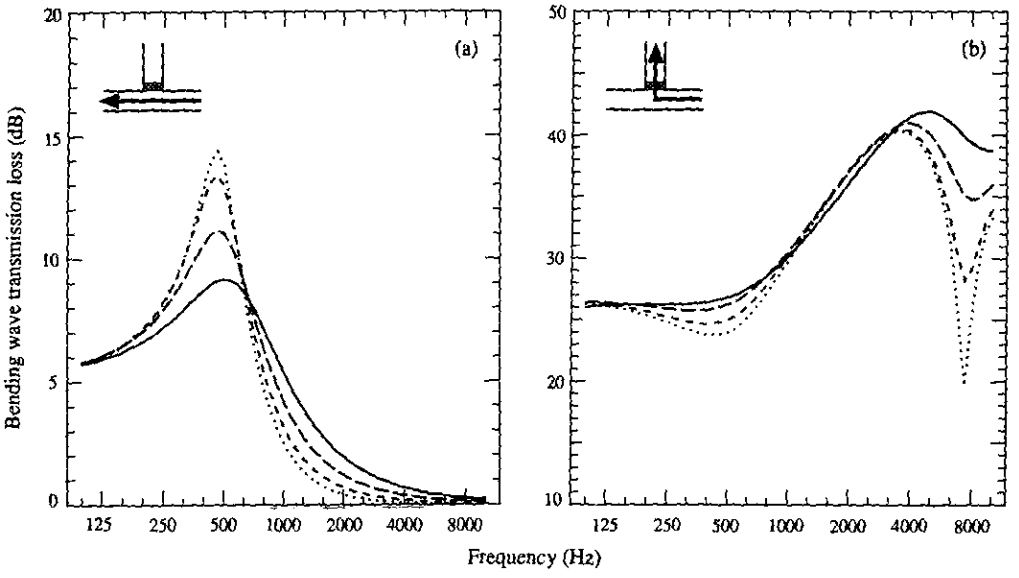

Figure 8. Predicted transmisson loss for an elastic junction with an offset of 1/2 the plate's thickness. Interlayer loss factor: · · · ·, $\eta_l = 0{\cdot}05$; - - - -, $\eta_l = 0{\cdot}2$; – – –, $\eta_l = 0{\cdot}5$; ——, $\eta_l = 1{\cdot}0$.

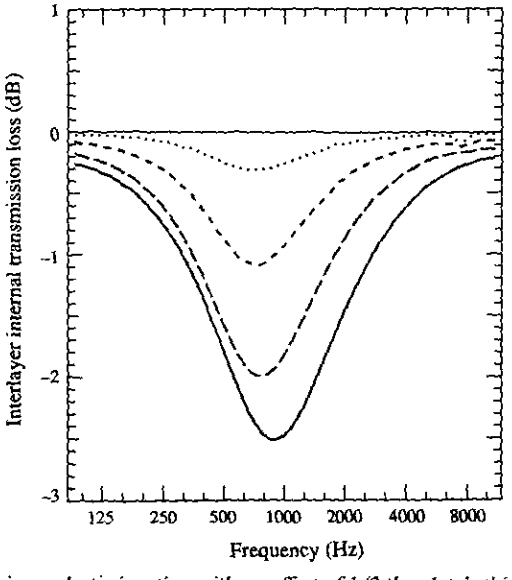

Figure 9. Internal losses in an elastic junction with an offset of 1/2 the plate's thickness. Interlayer loss factor: · · · ·, $\eta_l = 0{\cdot}05$; - - - -, $\eta_l = 0{\cdot}2$; – – –, $\eta_l = 0{\cdot}5$; ——, $\eta_l = 1{\cdot}0$.

interlayer contribute relatively little to the overall bending wave transmission loss; the main effect of the interlayer results from the decoupling of the plate motions.

4. FINITE ELEMENT SIMULATION FOR THE INTERLAYER

The analytical description of the dynamics of the interlayer is possible only for ideal displacement fields, as assumed in the preceding section. In any real application, the stress–strain condition in the interlayer will lie between the extremes presented in equations (15)

and (16). For a homogeneous, isotropic interlayer with its endplanes restrained against deformation, the apparent stiffness upon deformation will differ from the material stiffness, depending on the Poisson ratio of the material and on the geometry of the interlayer. For any specific geometry, this apparent stiffness can be calculated by using a finite element (FE) analysis of the interlayer. This approach has been used in the inverse problem, the determination of the elastic moduli of a material sample of a specific geometry [20].

The first idea in this research was to use an FE model of the interlayer as a "substructure" in the analytical model. The purpose of the FE analysis would be to calculate the transfer matrix $[T]$ of the interlayer. One or more elements (e.g., a column) of the transfer matrix could be calculated from the response of the interlayer upon a suitably chosen imposed displacement or force field at one side of the interlayer. Repeating this calculation for different imposed fields would yield all the elements of the matrix $[T]$. In practice, however, this approach becomes very cumbersome, because it requires a full analysis for every frequency as well as for every angle of incidence of the primary bending wave. Moreover, only a finite strip of the infinitely long interlayer can be modelled. This approach can therefore be envisaged only for a finite-sized interlayer, as would be the case for a junction between beams.

In the context of this study, the analysis is restricted to a two-dimensional simulation of the apparent stiffness of the interlayer. The procedure is as follows. A two-dimensional FE model of the cross-section of the interlayer is constructed. The endplanes are restricted against lateral motion because they can be assumed to be fixed against the plates. Two-dimensional plane strain solid elements are used in the model. A harmonic analysis is performed with one endplane fixed and the other endplane subjected to a plane longitudinal or transverse displacement, or to a plane rotation. An apparent compression, shear or bending modulus can be calculated from the ratio of the reaction forces or bending moment to the applied displacement or rotation. Alternatively, the apparent modulus can be calculated from the transfer function between both endplanes of the interlayer. This modulus is then introduced in the analytical model as a material property of the interlayer.

The results of an FE analysis for the case of an interlayer of 10 mm width and 1 and 4 mm thickness are shown in Figures 10 and 11. The plots show the apparent increase of the modulus of elasticity for the case of a longitudinal displacement or a rotation of the endplanes of the interlayer. The calculations are performed for a silicone interlayer with characteristics $\rho = 1050\ \text{kg/m}^3$ and $E = 2{\cdot}5$ MPa. The Poisson ratio is varied as $\nu = 0{\cdot}495$, $0{\cdot}49$, $0{\cdot}47$ and $0{\cdot}45$. It is observed that for nearly incompressible materials and for geometries with a low shape factor (ratio of thickness to width), the stiffening effect can become very important. Due to the different deformation conditions, this effect is more pronounced for the plane longitudinal displacement than for the plane rotation. For the interlayer of 1 mm thickness (see Figure 10), the effect depends little on frequency. For the interlayer of 4 mm thickness (see Figure 11), the effect becomes frequency dependent due to wave propagation.

5. EXPERIMENTAL SET-UP

In order to verify the theoretical results, the bending wave transmission loss was measured on a T-junction between plates with both rigid, hinged and elastic connections. The experimental set-up is shown in Figure 12. The rigid coplanar junction between plates 1 and 2 is formed by a horizontal plate. The third plate is vertically mounted in the middle, with varying connections to the horizontal plate. A rigid connection is achieved by mounting plate 3 by means of two aluminum profiles to the horizontal plate. A hinged connection is achieved by driving a strip of $0{\cdot}5$ mm thin band-steel into the edge of plate

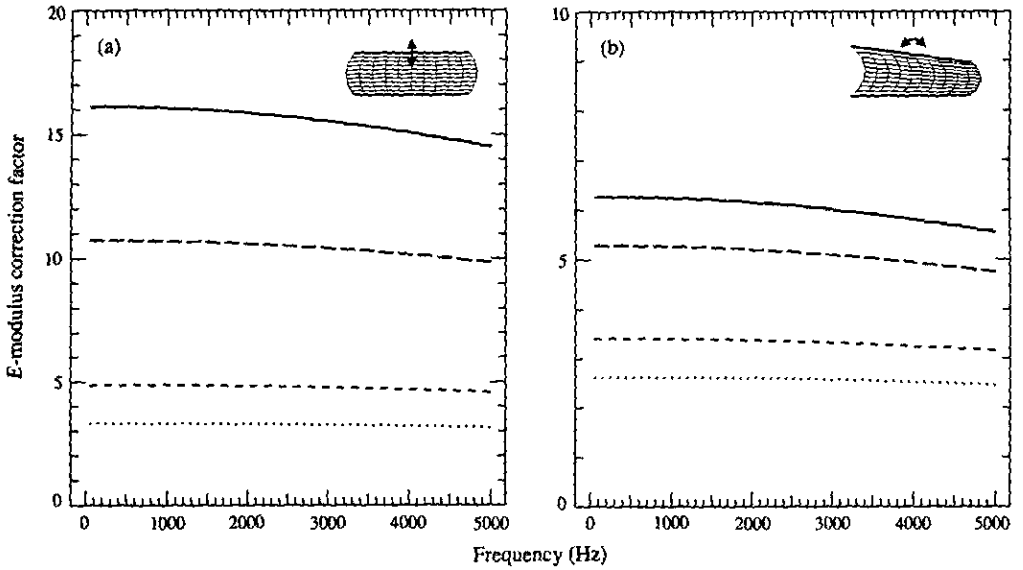

Figure 10. FE simulation of the correction factor for the modulus of elasticity of a $1 \times 10\,mm^2$ silicone interlayer. Interlayer Poisson ratio: ——, $\nu_l = 0{\cdot}495$; – – –, $\nu_l = 0{\cdot}49$; - - - -, $\nu_l = 0{\cdot}47$; · · · ·, $\nu_l = 0{\cdot}45$.

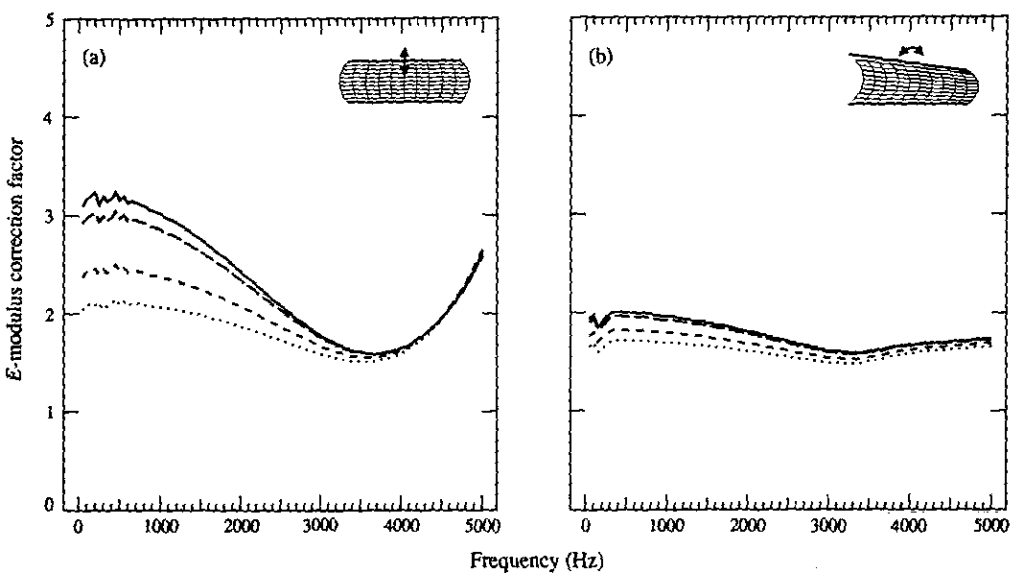

Figure 11. FE simulation of the correction factor for the modulus of elasticity of a $4 \times 10\,mm^2$ silicone interlayer. Interlayer Poisson ratio: ——, $\nu_l = 0{\cdot}495$; – – –, $\nu_l = 0{\cdot}49$; - - - -, $\nu_l = 0{\cdot}47$; · · · ·, $\nu_l = 0{\cdot}45$.

3, and then sliding this edge into a narrow slit on top of the horizontal plate. An elastic connection is obtained by applying a strip of silicone sealing on the horizontal plate, and then pressing the edge of plate 3 into it up to the desired thickness of the interlayer. After removal of the surplus of silicone and after drying, an interlayer is obtained that is glued perfectly to the edge of the plate. The whole set-up rests on two boxes through soft polyurethane strips.

A mechanical exciter is mounted on plate 1 not too close to the junction, and is fed with stationary white noise in the 100 Hz–10 kHz range. For each plate the r.m.s. acceleration

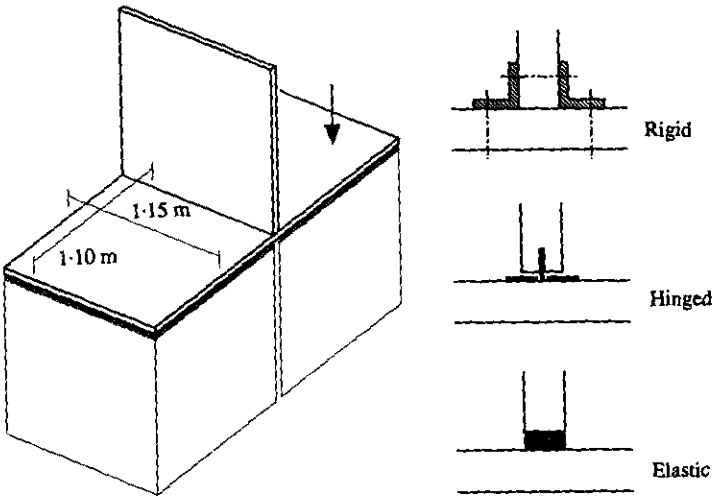

Figure 12. Measurement set-up, and details of the rigid, hinged and elastic junctions.

level L_A is determined from the measurement on 36 individual points on the plate surface using a lightweight accelerometer and a one-third octave real-time analyzer. The total damping η_i for each plate is derived from reverberation time measurements after interrupting the source mounted on the plate. From the measured data, the bending wave transmission loss is calculated as [21]

$$R_{ij} = L_{Ai} - L_{Aj} + 10 \log \left(\frac{2}{\pi \omega} c_{Bi} L_{ij} \frac{m_i}{m_j} \frac{1}{S_j} \frac{1}{\eta_{ij}} \right). \tag{24}$$

Equation (24) is derived from a statistical energy analysis (S.E.A.) of a subsystem of two plates i and j. This implies that the basic S.E.A. assumptions, as described for instance in the work of Lyon [22], are satisfied. Apart from the assumptions regarding the measurement formula, it is also assumed that the energy transmission between finite coupled plates can be derived from a diffuse wave transmission coefficient calculated with a theory based on semi-infinite plates. In doing so, several aspects such as the contribution of individual modes of the assembly or the contribution of nearfields to the vibration levels on the plates are neglected. These limitations can only be overcome by explicitly taking into account the finite dimensions of the plate structures, as done, for instance, in references [23]–[25]. For the evaluation of the measurement results in this study, these limiting assumptions should be borne in mind.

Additional measurements were made to determine the elastic constants of the materials used. The modulus of elasticity of the plate material is derived from measurements of the resonance frequencies of a free-free beam sample of the plate. The measurements are repeated for different orientations to check the isotropy of the plates. The Poisson ratio was taken from literature data. The modulus of elasticity of the interlayer is derived from measurements of the longitudinal wavespeed in small slender bars of rectangular cross-section. The dimensions of the samples are $60 \times 10 \times 10$ mm^3 and $60 \times 5 \times 5$ mm^3. The shear modulus of the interlayer is derived from measurements of the resonances of a mass-spring set-up. As a check, the Poisson ratio for static deformation was derived from the measurement of the lateral deformation of a material sample subjected to a static load.

6. EXPERIMENTAL RESULTS AND SIMULATIONS

Results for a hinged junction were obtained for a T-junction of woodboard plates. The dimensions and material characteristics are as follows: $d_p = 11{\cdot}5$ mm, $\rho_p = 640$ kg/m^3, $E_p = 4000$ MPa, $\nu_p = 0{\cdot}20$. A comparison between results for the rigid junction and the hinged junction is shown in Figure 13. At most measurement points, the coplanar bending wave transmission loss is slightly smaller for the case of the hinged junction, as predicted by the theory. The corner bending wave transmission loss is much higher in the case of a hinged junction. However, for both directions some measured values correspond poorly to the predictions. This can partly be explained by the orthotropy of the plates (E_p varying between 3000 and 5000 MPa) or by an incomplete contact of the hinge with the horizontal plate, especially for the higher frequencies.

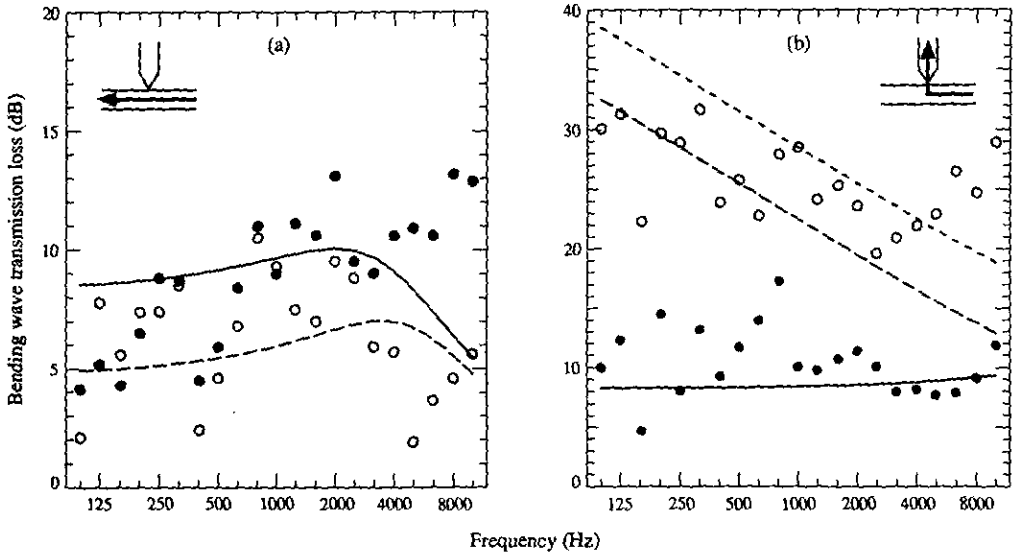

Figure 13. Transmission loss for a rigid and a hinged junction. ●, Measured rigid; ——, calculated rigid; ○, measured hinged; – – –, calculated hinged offset 5 mm; - - - - -, calculated hinged offset 2·5 mm.

Results for an elastic junction were obtained for a T-junction of PVC plates with an interlayer of silicone and an interlayer of polyurethane. The characteristics of the plates are $d_p = 10$ mm, $\rho_p = 1440$ kg/m^3, $E_p = 3580$ MPa and $\nu_p = 0{\cdot}35$. The characteristics of the silicone interlayer are $d_l = 1$, 2 and 4 mm, $\rho_l = 1050$ kg/m^3, $E_l = 2{\cdot}5$ MPa and $\nu_l = 0{\cdot}48$–$0{\cdot}50$. It was difficult to measure the Poisson ratio for the silicone, but it can be concluded that this material is almost incompressible. The characteristics of the polyurethane interlayer are $d_l = 4{\cdot}5$ mm, $\rho_l = 40$ kg/m^3, $E_l = 12$ MPa and $\nu_l = 0{\cdot}4$. The Poisson ratio for the polyurethane was derived from the stiffening effect, as observed for material samples of different geometries [20]. The simulations are performed with the stress–strain relationships for the interlayer as given in equations (23); the Poisson ratio is varied according to the values obtained from the finite element analysis described in the previous section.

The results for the elastic junctions with the silicone interlayer are shown in Figures 14–16. According to the finite element analysis, the interlayers of 1 mm and 2 mm thickness show a strong apparent stiffness; simulations are therefore performed with Poisson ratios of 0·47, 0·48 and 0·49. The interlayer of 4 mm thickness has a lower apparent stiffness; simulations are therefore performed with Poisson ratios of 0·40, 0·42 and 0·44. In all cases, the offset of the interlayer is taken to be half of the plate's thickness. The results for the

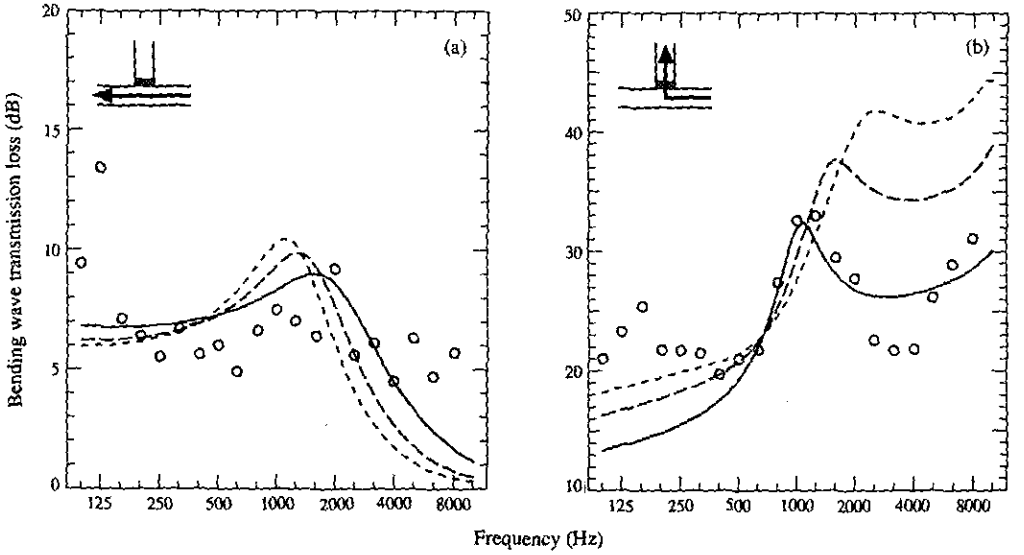

Figure 14. Transmission loss for an elastic junction of 1 mm silicone. ○, Measured; ——, calculated $\nu_l = 0{\cdot}49$; – – –, calculated $\nu_l = 0{\cdot}48$, - - - - -, calculated $\nu_l = 0{\cdot}47$.

interlayer of 1 mm thickness are shown in Figure 14, as is the effect of the stiffening. A value of $\nu_l = 0{\cdot}49$ seems to be optimal for this case. The results for the interlayer of 2 mm thickness are shown in Figure 15. For this case, the stiffening of the interlayer is still observed, although it is less apparent. The maximum in the coplanar junction damping is more pronounced and is shifted to the left. In the corner junction damping, the first shear resonance of the interlayer is visible. This phenomenon occurs at a frequency of approximately 7000 Hz, when the shear wavelength equals twice the interlayer thickness. The

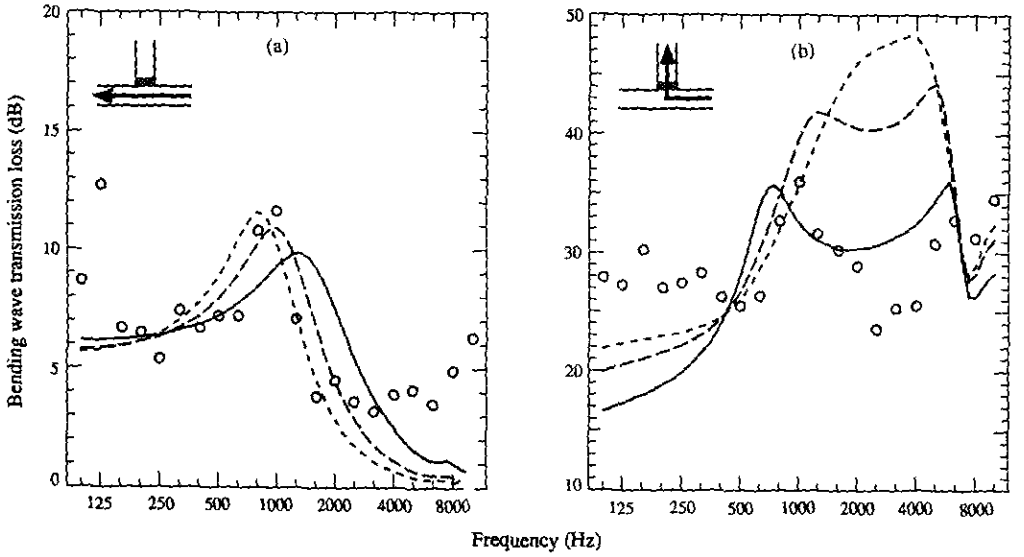

Figure 15. Transmission loss for an elastic junction of 2 mm silicone. ○, Measured; ——, calculated $\nu_l = 0{\cdot}49$; – – –, calculated $\nu_l = 0{\cdot}48$, - - - - -, calculated $\nu_l = 0{\cdot}47$.

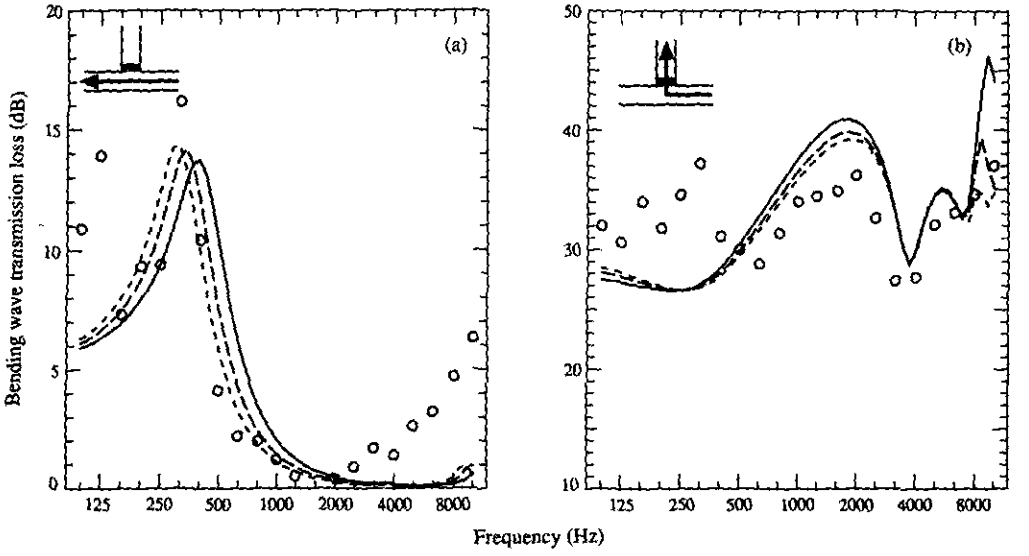

Figure 16. Transmission loss for an elastic junction of 4 mm silicone. O, Measured; ——, calculated $\nu_l = 0{\cdot}44$; – – –, calculated $\nu_l = 0{\cdot}42$, - - - - -, calculated $\nu_l = 0{\cdot}40$.

results for the interlayer of 4 mm thickness are shown in Figure 16. Here, the maximum in the coplanar junction damping is very pronounced and is further shifted to the lower frequencies. In the corner junction damping, the stiffening is no longer observed, but the influence of a shear resonance at 3500 Hz and at 7000 Hz is present.

The results for the elastic junction with the polyurethane interlayer are shown in Figure 17. The analysis was performed with a Poisson ratio of 0·3. The polyurethane is much stiffer and much lighter than the silicone. Due to this high stiffness, the maximum in the coplanar junction damping still occurs at a relatively high frequency, despite the lower

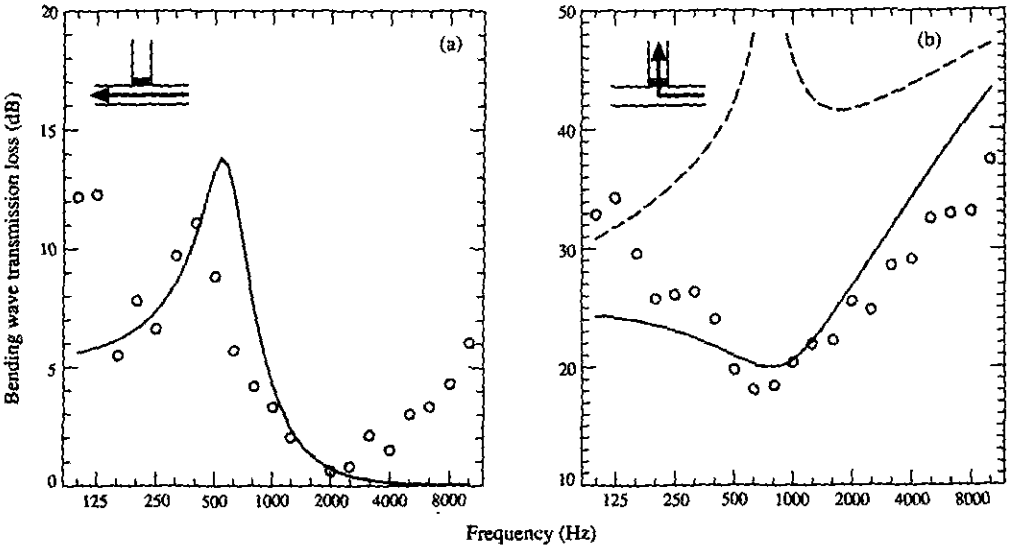

Figure 17. Transmission loss for an elastic junction of 4·5 mm polyurethane. O, Measured; ——, calculated offset 5 mm; – – –, calculated offset 0 mm.

Poisson ratio of the polyurethane. Due to the high wavespeed in the polyurethane interlayer, the influence of shear wave propagation in the corner junction damping is completely absent. Also shown in Figure 17 are the calculated results for the corner junction damping when a zero mounting offset for the interlayer is assumed. The observed discrepancy compared with the measurement results indicates that it is important to take this offset into account in equations (1)–(8) for the junction.

In general, the tendencies in the measurement results are fairly well predicted by the theory, although some problems remain. In the lower frequency range, the predicted transmission loss is often too low; this could be related to the finite dimensions of the plates and to the low modal density in this range. In the higher frequency range, the measured corner bending wave transmission loss for the case of an elastic interlayer (see Figures 14–16) often drops significantly below the theoretical predictions. We have no ready explanation for these deviations, but they could be related to an unobserved influence in the measurement set-up, or to a greater uncertainty about the material characteristics of the interlayer at higher frequencies.

7. CONCLUSIONS

A model has been presented for calculating the structure-borne sound transmission between plates connected by a hinge or by an elastic interlayer. The analytical model is based on the description of different wave types in the interlayer and in the semi-infinite plates. A two-dimensional finite element model is used to calculate a correction factor for the stiffening of the interlayer due to its restricted lateral contraction. The calculated and measured results demonstrate some important phenomena: the influence of the stiffening of the interlayer, the influence of an offset mounting of the hinge and the interlayer, and the influence of wave propagation in the interlayer. By using the model presented in the paper, other topics could be analyzed, including the influence of alternative placings of the interlayer, the influence of multiple interlayers in a junction, or the transmission of longitudinal and shear waves across elastic junctions and the attenuation provided over longer distances involving multiple junctions. However, in order to obtain reliable calculation results for junctions in practical situations, other important aspects, such as the finite dimensions of the plates, or a combination of elastic and rigid point or line connections, should be included in the theory.

REFERENCES

1. L. CREMER, M. HECKL and E. E. UNGAR 1988 *Structure-borne Sound*. Berlin: Springer-Verlag, second edition.
2. T. KIHLMAN 1967 *Report 9, National Swedish Institute for Building Research*. Transmission of structure-borne sound through buildings.
3. W. WÖHLE, TH. BECKMANN and H. SCHRECKENBACH 1981 *Journal of Sound and Vibration* **77**, 323–334. Coupling loss factors for statistical energy analysis of sound transmission at rectangular structural slab joints, part I.
4. W. WÖHLE, TH. BECKMANN and H. SCHRECKENBACH 1981 *Journal of Sound and Vibration* **77**, 335–344. Coupling loss factors for statistical energy analysis of sound transmission at rectangular structural slab joints, part II.
5. P. G. CRAVEN and B. M. GIBBS 1981 *Journal of Sound and Vibration* **77**, 417–427. Sound transmission and mode coupling at junctions of thin plates, part I: representation of the problem.
6. B. M. GIBBS and P. G. CRAVEN 1981 *Journal of Sound and Vibration* **77**, 429–435. Sound transmission and mode coupling at junctions of thin plates, part II: parametric survey.
7. W. WÖHLE 1990 *Acustica* **72**, 258–268. Körperschallübertragung in Gebäuden—Vergleich von Meßwerten mit Rechenergebnissen der Statistischen Energieanalyse.

8. B. M. GIBBS 1986 *Journal of Sound and Vibration* **104**, 127–136. Mode coupling and energy partition of sound in a system of plate junctions.
9. R. C. N. LEUNG and R. J. PINNINGTON 1990 *Journal of Sound and Vibration* **142**, 31–46. Wave propagation through right-angled joints with compliance-flexural incident wave.
10. S. GUDMUNDSSON 1984 *Report TVBA-3016, Lund Institute of Technology, Sweden.* Transmission of structure-borne sound at various types of junctions with thin elastic layers.
11. G. ROSENHOUSE and F. P. MECHEL 1985 *Proceedings of DAGA* 11, *Stuttgart* 1985, 399–402. Flanking through hinged joints of building elements as compared with fixed ones.
12. R. S. LANGLEY and K. H. HERON 1990 *Journal of Sound and Vibration* **143**, 241–253. Elastic wave transmission through plate/beam junctions.
13. M. D. MCCOLLUM and J. M. CUSCHIERI 1990 *Journal of the Acoustical Society of America* **88**(3), 1480–1485. Bending and in-plane wave transmission in thick connected plates using statistical energy analysis.
14. G. KURTZE, K. TAMM and S. VOGEL 1955 *Acustica* **5**, 223–233. Modellversuche zur Biegewellendämmung an Ecken.
15. G. ROSENHOUSE 1970 *Journal of Sound and Vibration* **67**, 469–486. Acoustic wave propagation in bent thin-walled wave guides.
16. B. M. GIBBS and J. D. TATTERSALL 1987 *Journal of Vibration, Acoustics, Stress and Reliability in Design* **109**, 348–355. Vibrational energy transmission and mode conversion at a corner junction of square section rods.
17. J. A. MOORE 1990 *Journal of the Acoustical Society of America* **88**(6), 2766–2776. Vibration transmission through frame or beam junctions.
18. J. L. HORNER and R. G. WHITE 1991 *Journal of Sound and Vibration* **147**, 87–103. Prediction of vibrational power transmission through bends and joints in beam-like structures.
19. L. M. BREKHOVSKIKH 1990 *Waves in Layered Media.* New York: Academic Press.
20. S. SIM and K.-J. KIM 1990 *Journal of Sound and Vibration* **141**, 71–82. A method to determine the complex modulus and Poisson's ratio of viscoelastic materials for FEM applications.
21. B. L. CLARKSON and M. F. RANKY 1984 *Journal of Sound and Vibration* **94**, 249–261. On the measurement of the coupling loss factor of structural connections.
22. R. LYON 1975 *Statistical Energy Analysis of Dynamical Systems.* Cambridge, Massachusetts: MIT Press.
23. Y. SHEN and B. M. GIBBS 1986 *Journal of Sound and Vibration* **105**, 73–90. An approximate solution for the bending vibrations of a combination of rectangular thin plates.
24. J. L. GUYADER, C. BOISSON, C. LESUEUR and P. MILLOT 1986 *Journal of Sound and Vibration* **106**, 289–310. Sound transmission by coupled structures: application to flanking transmission in buildings.
25. J. M. CUSCHIERI 1991 *Journal of the Acoustical Society of America* **87**(3), 1159–1165. Structural power-flow analysis using a mobility power flow approach of an L-shaped plate.

APPENDIX 1: INTERLAYER TRANSFER MATRICES

The interlayer transfer relation is of the form $[L]=[T][P]$, as given in equations (11)–(13). The elements of the transfer matrix are t_{ij} (row i, column j). In the case of an interlayer modelled as a spring, the non-zero elements of $[T]$ are

$$t_{ii}=1, \quad i=1,\ldots,8, \qquad t_{13}=-\frac{(1+\nu_l)(1-2\nu_l)}{E_l(1-\nu_l)}\frac{d_l}{h_p},$$

$$t_{24}=-\frac{2(1+\nu_l)}{E_l}\frac{d_l}{h_p}=t_{56}, \qquad t_{78}=\frac{(1+\nu_l)(1-2\nu_l)}{E_l(1-\nu_l)}\frac{12d_l}{h_p^3}.$$

In the case of an interlayer modelled as a wave medium, the non-zero elements of $[T]$ are

$$t_{11}=(1/k_L^2)[(1-\mu)k_z^2\cosh(jk_{Lx}d)+(\mu k_z^2+k_{Lx}^2)\cosh(jk_{Tx}d)],$$

$$t_{12}=(k_z/k_{Lx}k_T^2)[-(k_z^2-k_{Tx}^2)\sinh(jk_{Lx}d)-2k_{Lx}k_{Tx}\sinh(jk_{Tx}d)],$$

$$t_{13}=(jk_z/\sigma k_L^2)[\cosh(jk_{Lx}d)-\cosh(jk_{Tx}d)],$$

$$t_{14} = (j/\tau k_{Lx} k_T^2)[k_z^2 \sinh(jk_{Lx}d) + k_{Lx}k_{Tx} \sinh(jk_{Tx}d)],$$

$$t_{21} = (k_z/k_{Tx}k_L^2)[(1-\mu)k_{Lx}k_{Tx} \sinh(jk_{Lx}d) - (\mu k_z^2 + k_{Lx}^2) \sinh(jk_{Tx}d)],$$

$$t_{22} = (1/k_T^2)[-(k_z^2 - k_{Tx}^2) \cosh(jk_{Lx}d) + 2k_z^2 \cosh(jk_{Tx}d)],$$

$$t_{23} = (j/\sigma k_{Tx} k_L^2)[k_{Lx}k_{Tx} \sinh(jk_{Lx}d) + k_z^2 \sinh(jk_{Tx}d)],$$

$$t_{24} = (jk_z/\tau k_T^2)[\cosh(jk_{Lx}d) - \cosh(jk_{Tx}d)],$$

$$t_{31} = \{j\sigma k_z(1-\mu)(\mu k_z^2 + k_{Lx}^2)/k_L^2\}[-\cosh(jk_{Lx}d) + \cosh(jk_{Tx}d)],$$

$$t_{32} = (j\sigma/k_{Lx}k_T^2)[(k_z^2 - k_{Tx}^2)(\mu k_z^2 + k_{Lx}^2) \sinh(jk_{Lx}d) - 2k_z^2 k_{Lx}k_{Tx}(1-\mu) \sinh(jk_{Tx}d)],$$

$$t_{33} = (1/k_L^2)[(\mu k_z^2 + k_{Lx}^2) \cosh(jk_{Lx}d) + k_z^2(1-\mu) \cosh(jk_{Tx}d)],$$

$$t_{34} = (\sigma k_z/\tau k_{Lx} k_T^2)[(\mu k_z^2 + k_{Lx}^2) \sinh(jk_{Lx}d) - (1-\mu)k_{Lx}k_{Tx} \sinh(jk_{Tx}d)],$$

$$t_{41} = (j\tau/k_{Tx}k_L^2)[-2k_z^2 k_{Lx}k_{Tx}(1-\mu) \sinh(jk_{Lx}d) + (k_z^2 - k_{Tx}^2)(\mu k_z^2 + k_{Lx}^2) \sinh(jk_{Tx}d)],$$

$$t_{42} = \{j\tau 2k_z(k_z^2 - k_{Tx}^2)/k_T^2\}[\cosh(jk_{Lx}d) - \cosh(jk_{Tx}d)],$$

$$t_{43} = (\tau k_z/\sigma k_{Tx} k_L^2)[2k_{Lx}k_{Tx} \sinh(jk_{Lx}d) + (k_z^2 - k_{Tx}^2) \sinh(jk_{Tx}d)],$$

$$t_{44} = (1/k_T^2)[2k_z^2 \cosh(jk_{Lx}d) - (k_z^2 - k_{Tx}^2) \cosh(jk_{Tx}d)],$$

$$t_{55} = t_{66} = \cosh(jk_{Tx}d), \qquad t_{56} = (j/k_{Tx}d)/\{E/2(1+\nu)\} \sinh(jk_{Tx}d)$$

$$t_{65} = -jk_{Tx}d\{E/2(1+\nu)\} \sinh(jk_{Tx}d), \qquad t_{77} = t_{88} = \cosh(jk_{Lx}d),$$

$$t_{78} = -(12j/k_{Lx}h^3)/\{E(1-\nu)/(1+\nu)(1-2\nu)\} \sinh(jk_{Lx}d)$$

$$t_{87} = (jk_{Lx}h^3/12)\{E(1-\nu)/(1+\nu)(1-2\nu)\} \sinh(jk_{Lx}d)$$

In these expressions the subscripts l, referring to the interlayer, are dropped. Furthermore, the following abbreviations are used: $k_z = k_{Bl} \sin\theta_1$, $\mu = \nu/(1-\nu)$, $\sigma = \{E(1-\nu)/(1+\nu)(1-2\nu)\}h_p$ and $\tau = \{E/2(1+\nu)\}h_p$.

APPENDIX 2: NOTATION

A, B, C, D	wave amplitudes
c_B	bending wavespeed
R	bending wave transmission loss
d_l	thickness of interlayer l
e	mounting offset
E	modulus of elasticity
F_x, F_y, F_z	forces per unit width in x, y and z directions
G	shear modulus
h_p	thickness of plate p
k_B	bending wavenumber
k_L	longitudinal wavenumber
k_T	shear wavenumber
L_A	rms acceleration level
l_{ij}	coupling length between plate i and plate j
m	surface mass
S	surface area
M_z	bending moment per unit width around z-axis
x, y, z	local co-ordinate system of plate
x', y', z'	global co-ordinate system of plate assembly
$\xi_0, \eta_0, \zeta_0, \alpha_{z0}$	wave amplitudes of the junction beam
ξ	displacement along x-axis
η	displacement along y-axis

ζ	displacement along z-axis
α_z	rotation around z-axis
η_t	total loss factor
θ	for a plate, inclination angle; for a wave, incidence angle
ν	Poisson ratio
ρ	density
τ	bending wave transmission coefficient
Φ	potential
Ψ	scalar stream function
ω	circular frequency

Subscripts

1	referring to plate 1 (incident bending wave)
l	referring to interlayer l
p	referring to plate p
0	referring to the junction beam